International Journal of Marine Engineering Innovation and Research, Vol. 10(2), June. 2025. 287-296
(pISSN: 2541-5972, eISSN: 2548-1479)

Wave Diffraction and Independent Radiation by a Buoyant Body in Finite-Depth Water by Using an Exact NtD Boundary Condition

Un-Ryong Rim[1], Hyo-Song Ko[2], Gum-Chon Ri[3]
(Received: 12 March 2025 / Revised: 19 March 2025 /Accepted: 25 March 2025 / Available Online: 26 March 2025)

***Abstract*- Hydrodynamics of a floating structure is of interest from offshore and coastal engineers who develop the wave energy converters and utilize the marine space resources. Recently, Rim [1-3] proposed an exact DtN (Dirichlet-to-Neumann) artificial boundary condition in order to solve three-dimensional wave-structure interactions or wave motion over piecewise topographies numerically. This paper is concerned with another artificial boundary condition or so-called NtD (Neumann-to-Dirichlet) boundary condition in order to solve water wave diffraction and independent radiation by a buoyant body. A virtual cylindrical surface enclosing the floating body is chosen as a boundary on which an exact NtD map is analytically derived from a solution of the exterior subregion and then it is specified as a boundary condition in order to solve the interior problem. The present model shows good accuracy through the comparison with the DtN approach and suggests the escalated results for the effects of heading angle of incident wave and draft of a buoyant chamfer box.**

Keywords-- wave-structure interaction, floating body, boundary element method, NtD boundary condition

I. INTRODUCTION

Hydrodynamics of a floating structure is of interest from offshore and coastal engineers. Typical examples are: wave energy converters [4-7] to reduce the greenhouse gas emission [8,9]; offshore structures such as LNG (Liquefied Natural Gas) shuttle carriers or floating airports [10].

Analytical studies of wave diffraction and radiation problems have been suggested. Tyvand [11] focused on wave diffraction and independent radiation by a submerged circular in two-dimensional space cylinder by using a dimensionless parameter which is denoted as a ratio of radius and draft of the cylinder. Chatjigeorgiou [12,13] suggested analytical solutions expressed as a radial Mathieu function in order to solve a three-dimensional water wave diffraction problem by multiple cylinders with elliptical or circular cross-section which are bottom-mounted on a seabed. The whole velocity potential consists of incident water wave potential and wave diffraction potential due to the existence of circular cylinders and the wall. The wall is considered as a cylinder with elliptical section of fixed major axis and zero minor axis. Each component potential in the total potential is represented analytically by the modified Bessel functions and modified Mathieu functions in an elliptic coordinate system, where the unknowns in expression for each component potential are

Un-Ryong Rim, Institute of Ocean Engineering, Kim Chaek University of Technology, Pyongyang, Democratic People's Republic of Korea, Email: lur8971@star-co.net.kp
Hyo-Song Ko, Waudo District, Nampho City, Democratic People's Republic of Korea, khs9226@star-co.net.kp
Gum-Chon Ri, Department of Environmental Protection, Rajin University of Marine Transport, Chongjin, Democratic People's Republic of Korea, rgc911014@star-co.net.kp

obtained by using the matching method for eigenfunction expansion. Such an eigenfunction matching method has been widely used in order to obtain the other analytical solutions for wave-structure interaction problems [14-20]. The total water domain is divided into several subdomains and an analytical solution for velocity potential in the individual subdomain is expanded as a Fourier series in which the coefficients are determined by a matching condition on the interfaces between subdomains. Zheng et al. [21] focused on the two-dimensional water wave diffraction and independent water wave radiation by a rectangular structure floating in front of a wall by using the eigenfunction matching method. The total fluid domain is divided into several subdomains: first subdomain is between the structure and the wall; second subdomain is beneath the structure; and third subdomain is other rest region located seawards. The solution for each subdomain is analytically expressed in form of series by use of the variable separation approach and the unknown coefficients in the series can be determined by a continuity condition of velocity and pressure on the interfaces between subdomains. Meanwhile, Bhattacharjee and Soares [22] adopted such an approach to solve a wave diffraction by a structure floating over a step-type seabed in the two-dimensional space. Similar studies can also be found in Teng and Ning [23] and Teng et al. [24] for a bottom-mounted cylinder, Zheng and Zhang [25,26] for a floating cylinder, and Mavrakos et al. [27] for several floating cylinders, where the wave field in front of a wall is replaced into a horizontally-infinite wave field without the wall by the mirror-image principle [28]. Also, the approximate solution method of wave diffraction and independent radiation by several cylinders can be found [29,30], in which an exact solution of velocity potential field for each isolated cylinder is first obtained analytically and then the interference by another cylinder or the scattered water wave emanating from another cylinder is approximated as a planar wave based on assumption of much larger distances between the cylinders compared to the wavelength of water wave. It is noted that the analytical studies are all progressed in case of regular bodies, i.e. rectangular, circular or elliptical cylinders. Numerical and experimental methods have been proposed in order to cope with the case of irregular bodies. Gao et al. [31] adopted a numerical water wave tank with height of 0.8m, length of 14m and width of 0.1m to simulate a two-dimensional resonant motion of surface water wave around a rectangular structure floating over mild-slope seabed. Narayanan et al. [32] studied a two-dimensional behavior for a wake of a vertical cylinder near a wall by using a thin filament attached to the cylinder. Michele et al. [33] studied the optimal design for an array of several flap gates near a vertical wall by combining boundary element method with the principle of image. Later, Yuan et al. [34] adopted a three-dimensional panel method and the mirror-image method to study an effect of side wall on hydrodynamic characteristic of a ship moving forward with constant speed. Meanwhile, Sarkar et al. [35] studied an effect of straight coastal line on the characteristic of a flap WEC (Wave Energy Convertor) based on Green's boundary integral equation for a semi-infinite water domain. Tsay et al. [36] and Tsay and Liu [37] proposed a hybrid type of finite element model to solve wave diffraction, refraction and dissipation by offshore structures. The whole water domain is separated into a finite volume of interior subregion and the other infinite exterior subregion, where the interior subregion is meshed by finite element method while the exterior subregion provides analytical expressions for velocity potential. The principle of variation is then applied to match continuity condition of potential and its derivative on each interface of subdomains. On the other hand, the BEM (boundary element method) is adopted widely in order to determine the velocity potential by wave diffraction, scattering and radiation [38-40]. One of difficulties in implementing BEM is to solve the problem on how to specify a boundary condition as exactly as possible, especially, at the location far from the considered bodies. Several ways were proposed to cope with this difficulty. Eatock et al. [41] chose a virtual cylindrical surface in order to extract a finite volume of fluid domain from open sea and then supposed that the loop integral of velocity potential over the virtual surface is very close to zero when the distance between the virtual surface and the considered body is sufficiently long. Higdon [42,43] suggested an absorbing boundary condition so that the linear plane waves with

different speeds can transmit a virtual boundary without reflection. Such an approach can be found in other studies [44-46]. Meanwhile, Liao and Wong [47, 48] proposed multi-transmitting formulae (MTF) with an artificial speed and a spatial extrapolation in order to maintain the non-reflection of one-directional incident water waves with different propagation speeds on a virtual boundary. Chen and Liao [49] escalated such a method to the attenuating water waves. On the other hand, Shao and Faltinsen [50] made a damping zone in the vicinity of a virtual cylinder and proposed a damping formula on the damping zone in which the unknown damping coefficients are specified empirically. Xu and Duan [51] suggested a novel MTF on a damping zone in order to solve a three-dimensional hydrodynamic interaction between several floating bodies in spatial and time domains [52]. Chen and Liang [53] focused on a free-surface flow around floating bodies by use of a multi-domain approach in which the water domain is divided into an interior subdomain including the considered body, an exterior subdomain and a transit subdomain, where the viscosity of fluid and the nonlinearity of free water surface are considered in interior subdomain but the viscosity and nonlinearity are ignored and thus the linear potential theory is applied in the exterior subdomain. The Green function is adopted in the exterior subdomain to satisfy Sommerfeld radiation condition, free-surface boundary condition and the other boundary condition. Liang and Chen [54] adopted such an approach to determine the first and second-order drift wave loads acting on floating bodies. Recently, Rim [1-3] and Rim et al. [55-57] proposed an exact DtN (Dirichlet-to-Neumann) boundary condition to solve three-dimensional wave-structure interactions or wave motion over piecewise topographies numerically. This paper proposes a NtD boundary condition in order to solve water wave diffraction and independent radiation by a buoyant body in a finite-depth water region.

I. FORMULATION OF PROBLEM

A. Preliminaries

Focus on a body floating on water of finite depth h with an incident water wave with amplitude A, angular velocity ω and incident angle α as shown in Figure 1a, where the Oxy–plane is set on the still water surface while the positive direction of Oz–axis is upward. Under the assumption that the fluid is incompressible and inviscid and the flow is irrotational, the time-periodic wave field around the body can be written in terms of velocity potential as follows:

$$\phi(x,y,z,t) = \mathrm{Re}\left[\Phi(x,y,z;\omega)e^{-\mathrm{i}\omega t}\right], \quad (1)$$

where $\mathrm{i} = \sqrt{-1}$ is an imaginary unit and $\Phi(x,y,z;\omega)$ denotes an amplitude of ϕ can be written as $\Phi = \Phi_D + \Phi_R$ in which Φ_D and Φ_R are amplitudes of potentials due to wave diffraction by the fixed buoy and radiation by the oscillating buoy, respectively.

B. Wave diffraction

The diffraction potential Φ_D is composed of an incident potential Φ_I and a scattered potential Φ_S as follows:

$$\Phi_D(x,y,z;\omega) = \Phi_I(x,y,z;\omega) + \Phi_S(x,y,z;\omega). \quad (2)$$

The incident potential Φ_I is well-known as

$$\Phi_I(x,y,z;\omega) = -\frac{\mathrm{i}gA\cosh k_0(z+h)}{\omega\cosh k_0 h} e^{\mathrm{i}k_0(x\cos\alpha + y\sin\alpha)}, \quad (3)$$

where k_0 is called a wave number which satisfies the following dispersion relation $\omega^2 = gk_0\tanh k_0 h$. The potential Φ_S for a scattered

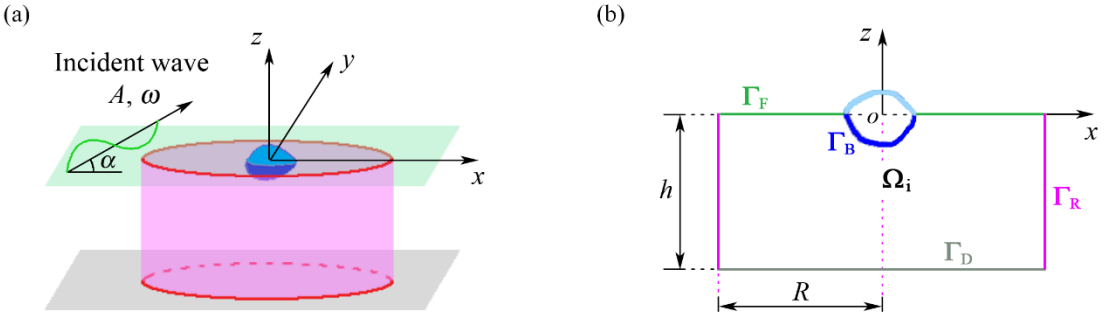

Figure 1. Problem definition (a) Perspective view of water wave region (b) Front view of interior subregion.

water wave satisfies the following governing equation and boundary conditions:

$$\frac{\partial^2 \Phi_S}{\partial x^2} + \frac{\partial^2 \Phi_S}{\partial y^2} + \frac{\partial^2 \Phi_S}{\partial z^2} = 0$$
everywhere in water region, (4)

$$\frac{\partial \Phi_S}{\partial z} - \frac{\omega^2}{g}\Phi_S = 0$$
on still water level $z = 0$, (5)

$$\frac{\partial \Phi_S}{\partial n} = -\frac{\partial \Phi_I}{\partial n}$$
on wetted part of the body surface, (6)

$$\frac{\partial \Phi_S}{\partial z} = 0 \text{ at seafloor } z = -h, \quad (7)$$

$$\sqrt{r}\left(\frac{\partial \Phi_S}{\partial r} - \mathrm{i}k_0\Phi_S\right) = 0 \text{ at } r \to \infty, \quad (8)$$

where $n = (n_x, n_y, n_z)$ means a unit vector normal to the body surface and pointing the inner part of water domain.

C. Wave radiation

The oscillatory motion of the floating body under the small amplitude wave can be denoted as $\xi_L(t) = \mathrm{Re}\left[\hat{\xi}_L e^{-\mathrm{i}\omega t}\right]$ by which the radiation potential Φ_R is then decomposed into

$$\Phi_R = \sum_{L=1}^{6}\left(-\mathrm{i}\omega\hat{\xi}_L\right)\Phi_L, \quad (9)$$

where $\hat{\xi}_L$ is an amplitude of L-th modal motion of the body and Φ_L is a complex amplitude of a radiation potential by the body oscillation in case of unit amplitude of L-th modal velocity, in which $L = \overline{1,6}$ means three translational modes and three rotational modes, i.e. six degrees-of-freedom (DOFs).

The potential Φ_L for the radiated water wave is specified by the following governing equation and boundary conditions:

$$\frac{\partial^2 \Phi_L}{\partial x^2} + \frac{\partial^2 \Phi_L}{\partial y^2} + \frac{\partial^2 \Phi_L}{\partial z^2} = 0 \text{ everywhere in water region,} \quad (10)$$

$$\frac{\partial \Phi_L}{\partial z} - \frac{\omega^2}{g}\Phi_L = 0 \text{ on still water level } z = 0, \quad (11)$$

$$\frac{\partial \Phi_L}{\partial n} = u_{n,L} \text{ on wetted part of the body surface,} \quad (12)$$

$$\frac{\partial \Phi_L}{\partial z} = 0 \text{ at seafloor } z = -h, \quad (13)$$

$$\sqrt{r}\left(\frac{\partial \Phi_L}{\partial r} - \mathrm{i}k_0\Phi_L\right) = 0 \text{ at } r \to \infty, \quad (14)$$

where $u_{n,L}$ denotes a normal component of velocity on the body surface when the body is under a L-th modal oscillation with unit amplitude of velocity.

D. Constitutive equations in the interior subregion

To numerically solve a hydrodynamic interaction between the incident water wave and the floating body in the confined water subregion with finite volume, an artificial circular cylinder Γ_R of radius R is adopted as seen in Figure 1, where the value of R has to be selected such that the artificial cylinder can include the body. Then the fluid domain is divided into an exterior subregion Ω_e and an interior subregion Ω_i, where Ω_i is surrounded by still water surface Γ_F, seabed Γ_D, the wetted surface of body Γ_B, and the artificial surface Γ_R as shown in Figure 1b while Ω_e is a rest part unbounded horizontally. The boundary conditions on Γ_R, Γ_B and Γ_D are already given in Equations (5)-(7) and (11)-(13), thus it is required to specify a boundary condition on Γ_R only to solve Φ_χ $(\chi = S, L)$ in Ω_i. The boundary condition on Γ_R can be set in form of $\Phi_\chi = \Lambda\frac{\partial \Phi_\chi}{\partial r}$, where Λ is called a Neumann-to-Dirichlet (NtD) operator since it maps the Neumann-type data on Γ_R into a Dirichlet-type value on a point of Γ_R, which will be further considered in the next section. The wave-interaction in the interior subregion can then be governed by

$$\frac{\partial^2 \Phi_\chi}{\partial x^2} + \frac{\partial^2 \Phi_\chi}{\partial y^2} + \frac{\partial^2 \Phi_\chi}{\partial z^2} = 0 \text{ in } \Omega_i, \quad (15)$$

$$\frac{\partial \Phi_\chi}{\partial z} - \frac{\omega^2}{g}\Phi_\chi = 0 \text{ on } \Gamma_F, \quad (16)$$

$$\frac{\partial \Phi_\chi}{\partial n} = \begin{cases} -\frac{\partial \Phi_I}{\partial n} & \text{if } \chi = S \\ u_{n,L} & \text{if } \chi = L \end{cases} \text{ on } \Gamma_B, \quad (17)$$

$$\frac{\partial \Phi_\chi}{\partial z} = 0 \text{ on } \Gamma_D, \quad (18)$$

$$\Phi_\chi = \Lambda\frac{\partial \Phi_\chi}{\partial r} \text{ on } \Gamma_R. \quad (19)$$

E. NtD artificial boundary condition

The NtD map on Γ_R can be obtained based on an analytical solution for Ω_e. The velocity potential in Ω_e is governed by

$$\frac{\partial^2 \Phi_\chi}{\partial x^2} + \frac{\partial^2 \Phi_\chi}{\partial y^2} + \frac{\partial^2 \Phi_\chi}{\partial z^2} = 0 \text{ in } \Omega_e, \quad (20)$$

$$\frac{\partial \Phi_\chi}{\partial z} - \frac{\omega^2}{g}\Phi_\chi = 0 \text{ on } z = 0 \text{ and } r \geq R, \quad (21)$$

$$\frac{\partial \Phi_\chi}{\partial z} = 0 \text{ on } z = -h \text{ and } r \geq R, \quad (22)$$

$$\sqrt{r}\left(\frac{\partial \Phi_\chi}{\partial r} - \mathrm{i}k_0\Phi_\chi\right) = 0 \quad \text{at } r \to \infty, \tag{23}$$

$$\frac{\partial \Phi_\chi}{\partial r} = \frac{\partial \Phi_\chi(R,\theta,z)}{\partial r} \quad \text{on } \Gamma_R, \tag{24}$$

where Equation (24) is called a Neumann boundary condition, i.e. it is assumed that the normal derivative of spatial potential on Γ_R is set as an already-specified function $\Xi(R,\theta,z)$ or $\frac{\partial \Phi_\chi(R,\theta,z)}{\partial r}$ intelligibly.

A general form of the solution satisfying Equations (20)-(23) can be expressed as [58,59]

$$\Phi_\chi(r,\theta,z) = \sum_{m=0}^{\infty}\{[a_{m0}H_m(k_0r)\cosh k_0(z+h) + \sum_{n=1}^{\infty} a_{mn}K_m(k_nr)\cos k_n(z+h)]\cos m\theta + [b_{m0}H_m(k_0r)\cosh k_0(z+h) + \sum_{n=1}^{\infty} b_{mn}K_m(k_nr)\cos k_n(z+h)]\sin m\theta\}, \tag{25}$$

and its radial derivative is expressed as

$$\frac{\partial \Phi_\chi(r,\theta,z)}{\partial r} = \sum_{m=0}^{\infty}\{[a_{m0}H_m'(k_0r)\cosh k_0(z+h) + \sum_{n=1}^{\infty} a_{mn}k_nK_m'(k_nr)\cos k_n(z+h)]\cos m\theta + [b_{m0}H_m'(k_0r)\cosh k_0(z+h) + \sum_{n=1}^{\infty} b_{mn}k_nK_m'(k_nr)\cos k_n(z+h)]\sin m\theta\}, \tag{26}$$

where $K_m(\cdot)$ is a modified second-kind Bessel function with order m (m = 0,1,2,...), $H_m(\cdot)$ is a first-kind Hankel function with order m, k_n ($n > 0$) denotes an eigenvalue with order n calculated by $\omega^2 = -gk_n\tan k_nh$, and the coefficients a_{mn} and b_{mn} are unknowns as for now and will be determined in the following paragraph.

Equation (26) is expressed as a type of Fourier series with θ, where the Fourier coefficients can be again expressed as a type of series composed of the following orthonormal functions with reference to z in a domain $[-h, 0]$:

$$Z_{k_n}(z) = \begin{cases} N_{k_0}^{-0.5}\cosh k_0(z+h), & n = 0 \\ N_{k_n}^{-0.5}\cos k_n(z+h), & n \neq 0 \end{cases} \tag{27}$$

where

$$N_{k_n} = \begin{cases} \frac{h}{2}\left(1 + \frac{\sinh 2k_0h}{2k_0h}\right), & n = 0 \\ \frac{h}{2}\left(1 + \frac{\sin 2k_nh}{2k_nh}\right), & n \neq 0 \end{cases} \tag{28}$$

Substituting $r = R$ into Equation (26) and from the boundary condition (24) on $r = R$, the unknown coefficients a_{mn} and b_{mn} can be expressed from Equation (27) as follows:

$$a_{mn} = \frac{N_{k_n}^{-0.5}}{\pi\varepsilon_m k_n F_m'(k_nR)}\int_{-h}^{0}\int_{0}^{2\pi}\frac{\partial \Phi_\chi(R,\theta',z')}{\partial r}Z_{k_n}(z')\cos m\theta'\,d\theta'dz' \tag{29}$$

$$b_{mn} = \frac{N_{k_n}^{-0.5}}{\pi\varepsilon_m k_n F_m'(k_nR)}\int_{-h}^{0}\int_{0}^{2\pi}\frac{\partial \Phi_\chi(R,\theta',z')}{\partial r}Z_{k_n}(z')\sin m\theta'\,d\theta'dz' \tag{30}$$

where

$$\varepsilon_m = \begin{cases} 2, & m = 0 \\ 1, & m \neq 0 \end{cases} \tag{31}$$

$$F_m(k_nr) = \begin{cases} H_m(k_0r), & n = 0 \\ K_m(k_nr), & n \neq 0 \end{cases} \tag{32}$$

and $F_m'(\cdot)$ is a derivative of $F_m(\cdot)$ while θ' and z' denote independent variables apparently different from θ and z.

The solution for the exterior subregion (20)-(24) is therefore obtained finally from Equations (25), (29) and (30) as follows:

$$\Phi_S(r,\theta,z) = \sum_{m=0}^{\infty}\sum_{n=0}^{\infty}\int_{-h}^{0}\int_{0}^{2\pi}\frac{F_m(k_nr)}{\pi\varepsilon_m k_n F_m'(k_nR)}Z_{k_n}(z)Z_{k_n}(z')\cos m(\theta-\theta')\frac{\partial \Phi_\chi(R,\theta',z')}{\partial r}d\theta'dz' \tag{33}$$

Substitution of $r = R$ into Equation (33) will result in a NtD artificial boundary condition on Γ_R as follows:

$$\Phi_S(R,\theta,z) = \Lambda\frac{\partial \Phi_S(R,\theta,z)}{\partial r} \sum_{m=0}^{\infty}\sum_{n=0}^{\infty}\int_{-h}^{0}\int_{0}^{2\pi}\lambda_{mn}(z,z',\theta-\theta')\frac{\partial \Phi_\chi(R,\theta',z')}{\partial r}d\theta'dz', \tag{34}$$

where $\lambda_{mn}(z,z',\theta-\theta')$ is a NtD kernel specified as

$$\lambda_{mn}(z,z',\theta-\theta') = \frac{F_m(k_nR)}{\pi\varepsilon_m k_n F_m'(k_nR)}Z_{k_n}(z)Z_{k_n}(z')\cos m(\theta-\theta'). \tag{35}$$

F. Numerical implementation with NtD boundary condition

The following integral equation for potential Φ_χ is constructed from the Green's second identity as follows:

$$2\pi\Phi_\chi(P) = \int_\Gamma \left[\Phi_\chi(Q)\frac{\partial G(P,Q)}{\partial n_Q} - \frac{\partial \Phi_\chi(Q)}{\partial n_Q}G(P,Q)\right]d\Gamma_Q, \quad (36)$$

where Γ denotes an entire boundary surface of Ω_i (i.e. $\Gamma = \Gamma_F + \Gamma_B + \Gamma_D + \Gamma_R$), P and Q are field and source points on Γ, respectively, n_Q denotes a unit normal vector to the surface Γ starting from a point Q, and G is a Green's function defind by

$$G(P,Q) = \frac{1}{r} = \frac{1}{|P-Q|}. \quad (37)$$

From the boundary conditions (16)-(19) and (34), the Equation (36) can be rearranged as

$$2\pi\Phi_\chi(P) - \left(D_{\Gamma_F+\Gamma_B+\Gamma_D}\Phi_\chi\right)(P) - \frac{\omega^2}{g}\left[\left(S_{\Gamma_F}\Phi_\chi\right)(P)\right] - \left(S_{\Gamma_R}\frac{\partial\Phi_\chi}{\partial r}\right)(P) - \sum_{m=0}^{\infty}\sum_{n=0}^{\infty}\int_{-h}^{0}\int_0^{2\pi}\lambda_{mn}(z,z',\theta-\theta')\left[\left(D_{\Gamma_R}\frac{\partial\Phi_\chi}{\partial r}\right)(P)\right]d\theta' dz' = \begin{cases}\left(S_{\Gamma_B}\frac{\partial\Phi_I}{\partial n}\right)(P) & \text{if } \chi = S\\ -\left(S_{\Gamma_B}u_{n,L}\right)(P) & \text{if } \chi = L\end{cases}, \quad (38)$$

where $S_\delta\psi$ and $D_\delta\psi$ denote operators or functionals of spatial function ψ defined on an arbitrary surface δ defined by

$$(S_\delta\psi)(P) = \int_\delta G(P,Q)\psi(Q)d\delta_Q \quad (39)$$

$$(D_\delta\psi)(P) = \int_\delta \frac{\partial G(P,Q)}{\partial n_Q}\psi(Q)d\delta_Q \quad (40)$$

Since Φ_I and $u_{n,L}$ in the right-handed side of Equation (38) are given already in Equation (3) and by preliminary set of L-th modal oscillatory motion of the floating body with unit amplitude of velocity, therefore the unkown quantities in the left-handed side of Equation (38), i.e. Φ_χ on $\Gamma_F + \Gamma_B + \Gamma_D$ and $\frac{\partial\Phi_\chi}{\partial r}$ on Γ_R can be solved by dividing the entire boundary Γ into a finite number of panels and by truncating the series in Equation (38).

After the unknown potentials Φ_χ ($\chi = S, L, D$) on Γ_F and Γ_B are determined from Equations (38), (2) and (3), the k-th ($k = \overline{1,6}$) components of time-periodic excitation force and radiation force by wave diffraction and radiation can be respectively expressed as

$$f_D^{(k)}(\omega,t) = \mathrm{Re}\left[F_D^{(k)}(\omega)e^{-\mathrm{i}\omega t}\right] \quad (41)$$

and

$$f_R^{(k)}(\omega,t) = \mathrm{Re}\left[F_R^{(k)}(\omega)e^{-\mathrm{i}\omega t}\right], \quad (42)$$

where $k = \overline{1,3}$ and $k = \overline{4,6}$ mean the x-, y- and z-components of the wave excitation/radiation force and its moment about the barycentre of body, respectively, and the amplitudes $F_D^{(k)}$ and $F_R^{(k)}$ are calculated by

$$F_D^{(k)}(\omega) = -\mathrm{i}\omega\rho\int_{\Gamma_B}\Phi_D(x,y,z;\omega)n_k d\Gamma, \quad (43)$$

$$F_R^{(k)}(\omega) = -\mathrm{i}\omega\rho\int_{\Gamma_B}\Phi_R(x,y,z;\omega)n_k d\Gamma = -\omega^2\rho\sum_{L=1}^{6}\hat{\xi}_L\int_{\Gamma_B}\Phi_L(x,y,z;\omega)n_k d\Gamma = \sum_{L=1}^{6}\omega^2\hat{\xi}_L\hat{\mu}_L^{(k)}(\omega) + \sum_{L=1}^{6}\mathrm{i}\omega\hat{\xi}_L\hat{v}_L^{(k)}(\omega). \quad (44)$$

Where

$$\hat{\mu}_L^{(k)}(\omega) = -\rho\mathrm{Re}\left[\int_{\Gamma_B}\Phi_L(x,y,z;\omega)n_k d\Gamma\right] \quad (45)$$

And

$$\hat{v}_L^{(k)}(\omega) = -\rho\omega\mathrm{Im}\left[\int_{\Gamma_B}\Phi_L(x,y,z;\omega)n_k d\Gamma\right] \quad (46)$$

denote k-th components of hydrodynamic coefficients, i.e. added mass for Equation (45) and damping coefficients for Equation (46), due to the L-th modal oscillatory motion of submerged structure with unit amplitude of velocity, respectively, and n_k is specified by $n_1 = n_x$, $n_2 = n_y$, $n_3 = n_z$, $n_4 = -(z-z_0)n_y + (y-y_0)n_z$, $n_5 = (z-z_0)n_x - (x-x_0)n_z$, $n_6 = -(y-y_0)n_x + (x-x_0)n_x$, where (x_0, y_0, z_0) denotes the coordinates of body center.

The time-periodic wave elevation due to the wave diffraction can be expressed by $\eta(x,y,\omega,t) = \mathrm{Re}\left[\hat{\eta}(x,y,\omega)e^{-\mathrm{i}\omega t}\right]$, where the complex amplitude $\hat{\eta}$ is calculated by

$$\hat{\eta}(x,y,\omega) = \frac{\mathrm{i}\omega}{g}\Phi_D(x,y,0;\omega). \quad (47)$$

II. RESULTS AND DISCUSSION

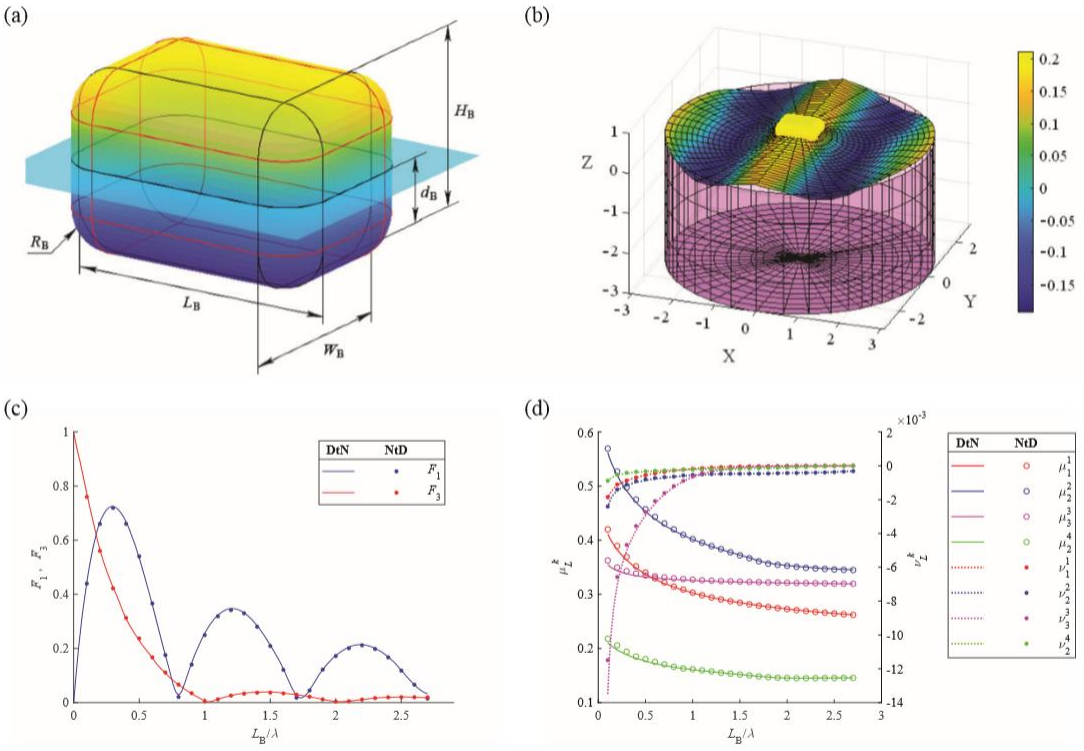

Figure 2. Comparison between DtN boundary condition [3,60] and NtD boundary condition (present) (a) A buoyant chamfer box with dimensions (b) Wave elevation around the chamfer box (c) Excitation forces; (d) Added mass and damping coefficients.

TABLE 1.
RELATIVE ERROR ACCORDING TO THE DIFFERENT VALUES OF *M* AND *N*

M	*N*	Relative error, %
3	2	21.87
5	4	11.95
7	5	6.87
9	7	4.52
11	8	3.28
14	10	2.59
17	15	2.25
21	18	2.12

A. Model validation

The NtD approach presented here is compared with a DtN model presented in Rim [3,60] which was fully validated through comparison with the analytical approach based on the eigenfunction expansion method. Figure 2a shows a buoyant chamfer box with L_B, W_B, H_B, d_B and R_B which denote length, width, height, draft and fillet radius, respectively. The results for the box with H_B/L_B =1.1, W_B/L_B =0.8, R_B/L_B =0.15, d_B/L_B =0.65 and h/L_B =3 are described in Figures 2b-d. Figure 2b shows the three-dimensional water wave elevation around the box at time $t = 2k\pi/\omega$ (k=0, 1, ...) under the incident water wave with A/L_B =0.2, L_B/λ =0.33 and $\alpha = 0°$, where λ is a wavelength determined from $\lambda = 2\pi/k_0$. Figure 2c shows the excitation forces acting to the box in case of $\alpha = 0°$, where the excitation forces are normalized by

$$F_k(\omega) = \left|F_D^{(k)}(\omega)\right| / \rho g A L_B W_B, \quad k=1, 3. \tag{48}$$

Figure 2d shows the hydrodynamic coefficients which are normalized by

$$\mu_L^{(k)}(\omega) = \begin{cases} \hat{\mu}_L^{(k)}(\omega)/\rho L_B W_B d_B, & L,k = 1,2,3 \\ \hat{\mu}_L^{(k)}(\omega)/\rho L_B W_B d_B^3, & L,k = 4,5,6 \\ \hat{\mu}_L^{(k)}(\omega)/\rho L_B W_B d_B^2, & else \end{cases} \tag{49}$$

and

$$v_L^{(k)}(\omega) = \begin{cases} \hat{v}_L^{(k)}(\omega)/\rho\omega L_B W_B d_B, & L,k = 1,2,3 \\ \hat{v}_L^{(k)}(\omega)/\rho\omega L_B W_B d_B^3, & L,k = 4,5,6 \\ \hat{v}_L^{(k)}(\omega)/\rho\omega L_B W_B d_B^2, & else \end{cases}. \quad (49)$$

Figures 2c and d show a little error (i.e. relative error less than 2.25%) between the results by the NtD method (present) and the DtN method [3,60], which is because the error might occur in meshing as wall as numerical calculation of Equation (38), but it will be reduced in case of denser mesh and increased number of truncated terms of the series in Equation (38). It is noted that the results presented in Figure 2 were obtained for $K = 36982$, $M = 17$ and $N = 15$, where K is the number of mesh elements on the boundary of interior subdomain, M and N denote the numbers of truncated terms in the series for m and n in Equation (38), respectively. The relative errors of the present results to the antecedent DtN method [3,60] are shown in Table 1 with different M and N. The convergent results in Table 1 show the validation of the present NtD approach.

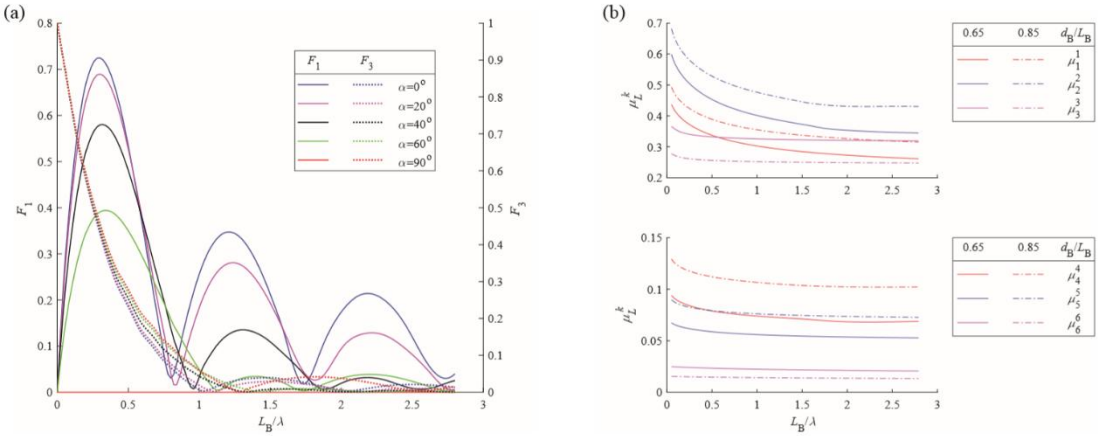

Figure 3. Effects of incident angle and draft (a) Effects of incident angle on excitation forces (b) Effects of draft on added mass.

B. Effects of some parameters

Figure 3 shows the effects of incident angle and draft on excitation forces and hydrodynamic coefficients. Figure 3a shows the effect of incident angle on excitation forces acting to the same chamfer box as in Figure 2 except that the incident angle is selected as $\alpha = 0°$, 20°, 40°, 60° and 90°, respectively. All plots of surge and heave forces versus L_B/λ in Figure 3a are less fluctuating and the peak points of surge force are lowering with the increment of α from 0° to 90°. It can also be found that the peak points in the plot of surge force for each α are lowering according to the increment of L_B/λ. Figure 3b shows the effect of draft on added mass of the same chamfer box as in Figure 2 except that the draft is selected as d_B/L_B =0.65 and 0.85$. All plots in Figure 3b are decreasing according to the increment of L_B/λ. It can also be found that the translational and rotational added masses in $x-$ and $y-$ directions in case of d_B/L_B =0.85 are greater than the results in case of d_B/L_B =0.65 while the translational and rotational added masses in $z-$ direction in case of d_B/L_B =0.85 are smaller than the results in case of d_B/L_B =0.65.

III. CONCLUSION

This paper aims to suggest a NtD boundary condition in order to solve water wave diffraction and independent radiation by a buoyant body in water of finite depth. A virtual cylindrical surface enclosing the floating body is chosen as a boundary on which an exact NtD map is analytically derived from a solution of the exterior subregion and then it is specified as a boundary condition in order to solve the interior problem. The present model

shows good accuracy through the comparison with the DtN approach [3,60]. The present NtD approach is extended to consider the effects of incident angle of the incident wave and draft of a buoyant chamfer box. All the plots of surge and heave forces for different incident angles are found to be less fluctuating and the peak points of surge force are lowering according to the increase of incident angle. And the translational and rotational added masses in $x-$ direction and $y-$ direction are found to be increasing according to the increment of draft while the translational and rotational added masses in $z-$ direction are found to be decreasing according to the increment of draft. The present NtD approach can be adopted to study the three-dimensional linear wave interaction with an arbitrarily-shaped floating body, and the nonlinear wave-structure interaction will be continued.

ACKNOWLEDGMENTS

The authors are grateful to the handling editor and anonymous reviewers with helpful comments.

REFERENCES

[1] U. R. Rim, "Numerical simulation for water wave motion over undulated seabed in front of a vertical wall by using an exact DtN boundary condition," Proceedings of 6th International Conference on Mathematics and Statistics, Leipzig, Germany, pp. 126–134, 2023. https://doi.org/10.1145/3613347.3613367

[2] U. R. Rim, "Wave interaction with multiple bodies bottom-mounted on an undulated seabed using an exact DtN artificial boundary condition," Journal of Ocean Engineering and Marine Energy, vol. 9, pp. 403–413, 2023. https://doi.org/10.1007/s40722-022-00275-6

[3] U. R. Rim, "Wave radiation by a floating body in water of finite depth using an exact DtN boundary condition," Journal of Ocean University of China, vol. 22, pp. 1497–1504, 2023. https://doi.org/10.1007/s11802-023-5358-2

[4] J. Abanades, G. Flor-Blanco, G. Flor, G. Iglesiasa, "Dual wave farms for energy production and coastal protection," Ocean and Coastal Management, vol. 160, pp. 18–29, 2018.

[5] D. Ning, Y. Zhou, C. Zhang, "Hydrodynamic modeling of a novel dual-chamber OWC wave energy converter," Applied Ocean Research, vol. 78, pp. 180–191, 2018.

[6] B. Zanuttigh, E. Angelelli, "Experimental investigation of floating wave energy converters for coastal protection purpose," Coastal Engineering, vol. 80, pp. 148–159, 2013.

[7] J. Cruz, "Ocean Wave Energy: Current Status and Future Perspectives," Springer-Verlag Berlin Heidelberg, Berlin, Germany, 2008.

[8] R. Atan, W. Finnegan, S. Nash, J. Goggins, "The effect of arrays of wave energy converters on the nearshore wave climate," Ocean Engineering, vol. 172, pp. 373–384, 2019.

[9] R. J. Bergillos, C. Rodriguez-Delgado, J. Allen, G. Iglesias, "Wave energy converter configuration in dual wave farms," Ocean Engineering, vol. 178, pp. 204–214, 2019.

[10] M. Lamas-Pardo, G. Iglesias, L. Carral, "A review of very large floating structures (VLFS) for coastal and offshore uses," Ocean Engineering, vol. 109, pp. 677–690, 2015.

[11] P. A. Tyvand, "Wave radiation and diffraction from a small submerged circular cylinder," Fluid Dynamics Research, vol. 9, pp. 279–288, 1992.

[12] I. K. Chatjigeorgiou, "Three dimensional wave scattering by arrays of elliptical and circular cylinders," Ocean Engineering, vol. 38, pp. 1480–1494, 2011.

[13] I. K. Chatjigeorgiou, "Semi-analytical solution for the water wave diffraction by arrays of truncated circular cylinders in front of a vertical wall," Applied Ocean Research, vol. 88, pp. 147–159, 2019.

[14] D. D. Bhatta, M. Rahman, "On scattering and radiation problem for a cylinder in water of finite depth," International Journal of Engineering Science, vol. 41, pp. 931–967, 2003.

[15] Y. Drobyshevski, "Hydrodynamic coefficients of a floating, truncated vertical cylinder in shallow water," Ocean Engineering, vol. 31, pp. 269–304, 2004.

[16] B. J. Wu, Y. H. Zheng, Y. G. You, D. S. Jie, Y. Chen, "On diffraction and radiation problem for two cylinders in water of finite depth," Ocean Engineering, vol. 33, pp. 679–704, 2006.

[17] P. Siddorn, R. Eatock-Taylor, "Diffraction and independent radiation by an array of floating cylinders," Ocean Engineering, vol. 35, pp. 1289–1303, 2008.

[18] W. Finnegan, M. Meere, J. Goggins, "The wave excitation forces on a truncated vertical cylinder in water of infinite depth," Journal of Fluids and Structures, vol. 40, pp. 201–213, 2013.

[19] X. Lu, K. H. Wang, "Modeling a solitary wave interaction with a fixed floating body using an integrated analytical-numerical approach," Ocean Engineering, vol. 109, pp. 691–704, 2015.

[20] K. Ren, G. X. Wu, C. Y. Ji, "Wave diffraction and radiation by a vertical circular cylinder standing in a three-dimensional polynya," Journal of Fluids and Structures, vol. 82, pp. 287–307, 2018.

[21] Y. H. Zheng, Y. M. Shen, Y. G. You, B. J. Wu, D. S. Jie, "On the radiation and diffraction of water waves by a rectangular structure with a sidewall," Ocean Engineering, vol. 31, pp. 2087–2104, 2004.

[22] J. Bhattacharjee, C. G. Soares, "Wave interaction with a floating rectangular box near a vertical wall with step type bottom topography," Journal of Hydrodynamics, vol. 22, pp. 91–96, 2010.

[23] B. Teng, D. Z. Ning, "Wave diffraction by a uniform cylinder in front of a vertical wall," Ocean Engineering, vol. 21, pp. 48–52, 2003.

[24] B. Teng, D. Z. Ning, X. T. Zhang, "Wave radiation by a uniform cylinder in front of a vertical wall," Ocean Engineering, vol. 31, pp. 201–224, 2004.

[25] S. Zheng, Y. Zhang, "Wave diffraction from a truncated cylinder in front of a vertical wall," Ocean Engineering, vol. 104, pp. 329–343, 2015.

[26] S. Zheng, Y. Zhang, "Wave radiation from a truncated cylinder in front of a vertical wall," Ocean Engineering, vol. 111, pp. 602–614, 2016.

[27] S. A. Mavrakos, G. M. Katsaounis, K. Nielsen, G. Lemonis, "Numerical performance investigation of an array of heaving power converters in front of a vertical breakwater," Proceedings of 14th International Offshore and Polar Engineering Conference, Toulon, France, pp. 238–245, 2004.

[28] B. W. Spring, P. L. Monkmeyer, "Interaction of plane waves with a row of cylinders," Civil Engineering in the Oceans, vol. 3, pp. 979–998, 1975.

[29] A. N. Williams, A. G. Abul-Azm, "Hydrodynamic interactions in floating cylinder arrays–ii. wave radiation," Ocean Engineering, vol. 16, pp. 217–263, 1989.

[30] A. N. Williams, Z. Demirbilek, "Hydrodynamic interactions in floating cylinder arrays – I. wave scattering," Ocean Engineering, vol. 15, pp. 549–583, 1988.
[31] J. Gao, Z. He, J. Zang, Q. Chen, H. Ding, G. Wang, "Topographic effects on wave resonance in the narrow gap between fixed box and vertical wall," Ocean Engineering, vol. 180, pp. 97–107, 2019.
[32] K. V. Narayanan, S. Vengadesan, K. Murali, "Wall proximity effects on the flow past cylinder with flexible filament," Ocean Engineering, vol. 157, pp. 54–61, 2018.
[33] S. Michele, P. Sammarco, M. Errico, "The optimal design of a flap gate array in front of a straight vertical wall: Resonance of the natural modes and enhancement of the exciting torque," Ocean Engineering, vol. 118, pp. 152–164, 2016.
[34] Z. M. Yuan, X. Zhang, C. Y. Ji, L. Jia, H. Wang, A. Incecik, "Side wall effects on ship model testing in a towing tank," Ocean Engineering, vol. 147, pp. 447–457, 2018.
[35] D. Sarkar, E. Renzi, F. Dias, "Effect of a straight coast on the hydrodynamics and performance of the oscillating wave surge converter," Ocean Engineering, vol. 105, pp. 25–32, 2015.
[36] T. K. Tsay, W. Zhu, P. L. F. Liu, "A finite element model for wave refraction, diffraction, reflection and dissipation," Applied Ocean Research, vol. 11, pp. 33–38, 1989.
[37] T. K. Tsay, P. L. F. Liu, "A finite element model for wave refraction and diffraction," Applied Ocean Research, vol. 5, pp. 30–37, 1983.
[38] B. Teng, R. Eatock-Taylor, "New higher-order boundary element methods for wave diffraction/radiation," Applied Ocean Research, vol. 17, pp. 71–77, 1995.
[39] C. G. Politis, M. V. Papalexandris, G. A. Athanassoulis, "A boundary integral equation method for oblique water-wave scattering by cylinders governed by the modified Helmholtz equation," Applied Ocean Research, vol. 24, pp. 215–233, 2002.
[40] J. Singh, A. Babarit, "A fast approach coupling boundary element method and plane wave approximation for wave interaction analysis in sparse arrays of wave energy converters," Ocean Engineering, vol. 85, pp. 12–20, 2014.
[41] T. R. Eatock, S. M. Hung, F. P. Chau, "On the distribution of second order pressure on a vertical circular cylinder," Applied Ocean Research, vol. 11, pp. 183–193, 1989.
[42] R. L. Higdon, "Absorbing boundary conditions for difference approximations to the multi-dimensional wave equation," Mathematics and Computations, vol. 47, pp. 437–459, 1986.
[43] R. L. Higdon, "Numerical absorbing boundary conditions for the wave equation," Mathematics and Computations, vol. 49, pp. 65–90, 1987.
[44] R. L. Higdon, "Absorbing boundary conditions for acoustic and elastic waves in stratified media," Journal of Computational Physics, vol. 101, pp. 386–418, 1992.
[45] J. R. Dea, "Improving the performance of Higdon non-reflecting boundary conditions by using weighted differencing," Applied Numerical Mathematics, vol. 61, pp. 1186–1197, 2011.
[46] J. R. Dea, "Absorbing boundary conditions for the fractional wave equation," Applied Mathematics and Computation, vol. 219, pp. 9810–9820, 2013.
[47] Z. P. Liao, "Extrapolation non-reflecting boundary conditions," Wave Motion, vol. 24, pp. 117–138, 1996.
[48] Z. P. Liao, H. L. Wong, "A transmitting boundary for the numerical simulation of elastic wave propagation," Soil Dynamics and Earthquake Engineering, vol. 3, pp. 174–183, 1984.
[49] S. L. Chen, Z. P. Liao, "Multi-transmitting formula for attenuating waves," Acta Seismologica Sinica, vol. 16, pp. 283–291, 2003.
[50] Y. L. Shao, O. M. Faltinsen, "Use of body-fixed coordinate system in analysis of weakly nonlinear wavebody problems," Applied Ocean Research, vol. 32, pp. 20–33, 2010.
[51] G. Xu, W. Y. Duan, "Time-domain simulation of wave-structure interaction based on multi-transmitting formula coupled with damping zone method for radiation boundary condition," Applied Ocean Research, vol. 42, pp. 136–143, 2013.
[52] W. Y. Duan, J. K. Chen, B. B. Zhao, "Second-order Taylor expansion boundary element method for the second-order wave diffraction problem," Engineering Analysis with Boundary Elements, vol. 58, pp. 140–150, 2015.
[53] X. Chen, H. Liang, "Wavy properties and analytical modeling of free-surface flows in the development of the multi-domain method," Journal of Hydrodynamics, vol. 28, pp. 971976, 2016.
[54] H. Liang, X. Chen, "A new multi-domain method based on an analytical control surface for linear and second-order mean drift wave loads on floating bodies," Journal of Computational Physics, vol. 347, pp. 506532, 2017.
[55] U. R. Rim, G. H. Choe, N. H. Ri, M. H. Jon, W. S. Pae, U. H. Han, "An exact DtN artificial boundary condition for motion analysis of water wave with undulated seabed," Wave Motion, vol. 116, pp. 103063, 2023. https://doi.org/10.1016/j.wavemoti.2022.103063
[56] U. R. Rim, P. S. Dong, C. G. Jang, "Free surface wave interaction with a submerged body using a DtN boundary condition," Theoretical and Computational Fluid Dynamics, vol. 38, pp. 75–87, 2024. https://doi.org/10.1007/s00162-023-00682-x
[57] U. R. Rim, Y. G. Ri, W. C. Do, P. S. Dong, C. W. Kim, J. S. Kim, "Wave diffraction and radiation by a fully-submerged body in front of a vertical wall by using an exact DtN artificial boundary condition," Engineering Analysis with Boundary Elements, vol. 151, pp. 19–29, 2023. https://doi.org/10.1016/j.enganabound.2023.02.053
[58] P. S. Dong, U. R. Rim, "Wave interaction with a bottom-mounted body in front of a vertical wall using an exact DtN boundary condition," Iran Journal of Science and Technology – Transactions of Civil Engineering, vol. 48, pp. 3697-3705, 2024. https://doi.org/10.1007/s40996-024-01361-5
[59] G. J. Kim, S. H. Kim, U. R. Rim, M. H. Jon, "Hydrodynamic interaction of a floating structure with free water surface wave near a vertical wall based on a Dirichlet-to-Neumann (DtN) boundary condition," Marine Systems and Ocean Technology, vol. 20, pp. 18, 2025. https://doi.org/10.1007/s40868-024-00159-4
[60] U. R. Rim, "Wave diffraction by floating bodies in water of finite depth using an exact DtN boundary condition," Ocean Engineering, vol. 239, pp. 109711, 2021. https://doi.org/10.1016/j.oceaneng.2021.109711